Journal of Biomechanics 49 (2016) 2321–2330

Contents lists available at ScienceDirect

Journal of Biomechanics

journal homepage: www.elsevier.com/locate/jbiomech
www.JBiomech.com

A novel chemo-mechano-biological model of arterial tissue growth and remodelling

Pedro Aparício [a], Mark S. Thompson [a], Paul N. Watton [b,c,*]

[a] Institute of Biomedical Engineering, Department of Engineering Science, University of Oxford, UK
[b] Department of Computer science, University of Sheffield, Sheffield, UK
[c] INSIGNEO Institute for in silico Medicine, University of Sheffield, Sheffield, UK

ARTICLE INFO

Article history:
Accepted 18 April 2016

Keywords:
Mechanobiology
Remodelling
Collagen
Fibroblast
TGF-beta
Aneurysm
Mathematical model

ABSTRACT

Arterial growth and remodelling (G&R) is mediated by vascular cells in response to their chemical and mechanical environment. To date, mechanical and biochemical stimuli tend to be modelled separately, however this ignores their complex interplay. Here, we present a novel mathematical model of arterial chemo-mechano-biology. We illustrate its application to the development of an inflammatory aneurysm in the descending human aorta.

The arterial wall is modelled as a bilayer cylindrical non-linear elastic membrane, which is internally pressurised and axially stretched. The medial degradation that accompanies aneurysm development is driven by an inflammatory response. Collagen remodelling is simulated by adaption of the natural reference configuration of constituents; growth is simulated by changes in normalised mass-densities. We account for the distribution of attachment stretches that collagen fibres are configured to the matrix and, innovatively, allow this distribution to remodel. This enables the changing functional role of the adventitia to be simulated. Fibroblast-mediated collagen growth is represented using a biochemical pathway model: a system of coupled non-linear ODEs governs the evolution of fibroblast properties and levels of key biomolecules under the regulation of Transforming Growth Factor (TGF)-β, a key promoter of matrix deposition.

Given physiologically realistic targets, different modes of aneurysm development can be captured, while the predicted evolution of biochemical variables is qualitatively consistent with trends observed experimentally. Interestingly, we observe that increasing the levels of collagen-promoting TGF-β results in arrest of aneurysm growth, which seems to be consistent with experimental evidence. We conclude that this novel Chemo-Mechano-Biological (CMB) mathematical model has the potential to provide new mechanobiological insight into vascular disease progression and therapy.

1. Introduction

The arterial wall is a highly dynamic tissue. In response to changing environmental conditions, its properties can change in an attempt to restore a healthy/*homeostatic* state (Humphrey, 2008). Understanding the responses of vascular cells to such perturbations is essential to understand the growth and remodelling (G&R) of tissue and thus predict the evolution of vascular diseases such as genetic hereditary conditions (Lindsay and Dietz, 2011), atherosclerosis (Montecucco and Mach, 2009) or aneurysms (Sakalihasan et al., 2005). For instance, fibroblasts in the adventitia, and smooth muscle cells in the media, are highly sensitive to the properties of their surrounding environment: the fibrous, load-bearing matrix is a channel for transmission of mechanical stimuli (Chiquet et al., 2003); in the interstitial fluid, biochemical signals are relayed via diffusible signalling molecules (Leask, 2010).

Several computational models of arterial adaption during disease evolution have been developed (Baek et al., 2006; Volokh and Vorp, 2008; Watton et al., 2009). To date, such models have focussed on predicting the geometrical evolution of the arterial wall by coupling altered vascular mechanics to microstructural changes (Wilson et al., 2012; Balakhovsky et al., 2014). However, the chemo-biological mechanisms behind homeostasis maintenance or impairment in disease are not explicitly modelled. Conversely, in the cell biology and biochemistry communities,

* Corresponding author at: Insigneo Institute for *in silico* Medicine, The Pam Liversidge Building, Sir Frederick Mappin Building, Mappin Street, Sheffield S1 3JD Sheffield, UK. Tel.: +44 114 2226076.
E-mail addresses: pedro.aparicio@eng.ox.ac.uk (P. Aparício), mark.thompson@eng.ox.ac.uk (M.S. Thompson), p.watton@sheffield.ac.uk (P.N. Watton).

http://dx.doi.org/10.1016/j.jbiomech.2016.04.037

numerous models of the signalling pathways governing cell-to-cell communication and production of active species exist, e.g. McDougall et al. (2006) and Warsinske et al. (2015). However, these models do not consider mechanical stimuli.

We propose a novel Chemo-Mechano-Biological (CMB) mathematical model to describe the interdependent chemical, mechanical and biological states of the arterial wall. Our model builds on the mechanobiological model of Watton et al. (2009) by coupling it with a representation of the biochemical signalling networks of collagenous tissue G&R based on the model of Dale et al. (1996). Moreover, we explicitly model the changing functional role of the adventitia from a protective sheath to playing a load bearing role in aneurysms. This is achieved by modelling a distribution of collagen attachment stretches and proposing that the (homeostatic) distribution can adapt, Section 2. The model is parameterised to the descending human aorta (Appendix A.3). We illustrate the application of the model (Section 3) to simulate the evolution of an inflammatory aneurysm (Study 1), and its response to pharmacological intervention, i.e. the effects of applying a collagen-promoting drug to an enlarging aneurysm (Study 2). Our coupled CMB model is a first step towards investigating the evolution of diseased arteries on both mechanical and biochemical levels, as well as their response to pharmacological therapy.

2. Methods

Our CMB model integrates two published mathematical models, i.e. Watton et al. (2009) and Dale et al. (1996); see Fig. 1. The biochemical model of Dale et al. (1996) focusses on the temporal variation of cellular and molecular species relevant to collagen synthesis and degradation in the context of wound healing, however without considering the influence of system biomechanics on cell response. The signalling pathways biochemical model component formulated in Section 2.2 is an adaptation and extension of this model, cf. Fig. 1 (left).

2.1. Model formulation I: Biomechanical model

We model the artery as a two layered cylindrical non-linear elastic membrane. The derivation of the force-balance equation (FBE) governing the system's mechanics follows Watton et al. (2009). Let subscripts $L=M,A$ denote medial and adventitial layers, resp., and let superscripts $p=E,C$ denote elastin and collagen constituents, resp. Considering that the only load-bearing constituents are elastin and collagen in the media, and collagen in the adventitia, it follows

$$p=\frac{1}{R\lambda\lambda_z}\left[H_M\cdot\left(P_M^E(\lambda)+P_M^C(\lambda_M^C)\right)+H_A\cdot P_A^C(\lambda_A^C)\right], \tag{1}$$

where R is the unloaded inner radius; H_M,H_A the unloaded layer thicknesses; λ_z, λ the axial and circumferential stretches, resp.; p the internal pressure; and P_L^p, λ_L^p the 1st Piola–Kirchhoff stress term and stretch, resp., ofconstituent p in layer L. The medial elastinous constituent is modelled as a neo-Hookean material, and thus

$$P_M^E(\lambda)=m_M^E\cdot K_M^E\cdot\lambda\cdot\left(1-\frac{1}{\lambda_z^2\cdot\lambda^4}\right) \tag{2}$$

where $K_M{}^E$ is a stiffness-like material constant and $m_M^E(t)$ is the (dimensionless) normalised mass density of elastin.

We assume that collagen fibres have a distribution of recruitment stretches (see Watton et al., 2004, 2009 for details), with each fibre displaying a linear mechanical response, i.e.

$$\tilde{\Psi}_L^C(\lambda_L^C)=\begin{cases}0 & \lambda_L^C<1\\ \frac{K_L^C}{2}\cdot\left(\lambda_L^C-1\right)^2 & \lambda_L^C\geq 1\end{cases}, \tag{3}$$

where $K_L{}^C$ are stiffness-like material constants. In this study, for simplicity, we consider all collagen fibres to be circumferentially aligned. The strain energy density function (SEDF) for the entire collagenous tissue is obtained by integrating the fibre SEDF over the distribution of fibre recruitment stretches (Hill et al., 2012),

$$\Psi_L^C(\lambda)=\int_1^{\lambda}\tilde{\Psi}_L^C(\lambda_L^C)\cdot\rho\left(\lambda_L^R\right)\,d\lambda_L^R, \tag{4}$$

where circumferential (λ), collagen fibre ($\lambda_L{}^C$) and collagen recruitment ($\lambda_L{}^R$) stretches are related by $\lambda=\lambda_L^C\cdot\lambda_L^R$, and $\rho\left(\lambda_L^R\right)$ is the probability density function (pdf) characterising the distribution of collagen recruitment stretches in the population of fibres. We use a triangular distribution function (Chen, 2014), see Fig. 2,

$$\rho\left(\lambda_L^R\right)=\begin{cases}0 & \lambda_L^R<\lambda_L^{R,\min}\\ \frac{2\left(\lambda_L^R-\lambda_L^{R,\min}\right)}{\left(\lambda_L^{R,\max}-\lambda_L^{R,\min}\right)\left(\lambda_L^{R,mode}-\lambda_L^{R,\min}\right)} & \lambda_L^{R,\min}<\lambda_L^R<\lambda_L^{R,mode}\\ \frac{2\left(\lambda_L^{R,\max}-\lambda_L^R\right)}{\left(\lambda_L^{R,\max}-\lambda_L^{R,\min}\right)\left(\lambda_L^{R,\max}-\lambda_L^{R,mode}\right)} & \lambda_L^{R,mode}<\lambda_L^R<\lambda_L^{R,\max}\\ 0 & \lambda_L^R>\lambda_L^{R,\max}\end{cases}. \tag{5}$$

where $\lambda_L^{R,\min}$ and $\lambda_L^{R,\max}$ define the minimum and maximum collagen recruitment stretches for the distribution resp., i.e. minimum/maximum factors' tissue much be stretch for collagen fibres of maximum/minimum undulation to begin to bear load; $\lambda_L^{R,mode}$ relates to the modal recruitment stretch of the distribution.

The stress term for the entire distribution of collagenous fibres in each layer L is obtained by multiplying the SEDF (Eq. (4)) by the respective normalised mass density term and subsequent partial differentiation with respect to λ, i.e.

$$P_L^C(\lambda_L^C)=\frac{\partial m_L^C\Psi_L^C}{\partial\lambda}=m_L^C\cdot\left(\frac{\partial}{\partial\lambda}\int_1^{\lambda}\tilde{\Psi}_L^C(\lambda)\cdot\rho\left(\lambda_L^R\right)\,d\lambda_L^R\right) \tag{6}$$

where $m_L{}^C$ denote collagen normalised mass densities in layer L. The derivation of the explicit form of Eq. (6) can be found in Appendix A.1. The normalised mass densities of the structural constituents medial elastin $m_M{}^E$, medial collagen $m_M{}^C$ and adventitial collagen $m_A{}^C$ are computed by Eqs. (8) and (12), resp., in the signalling pathways model component below.

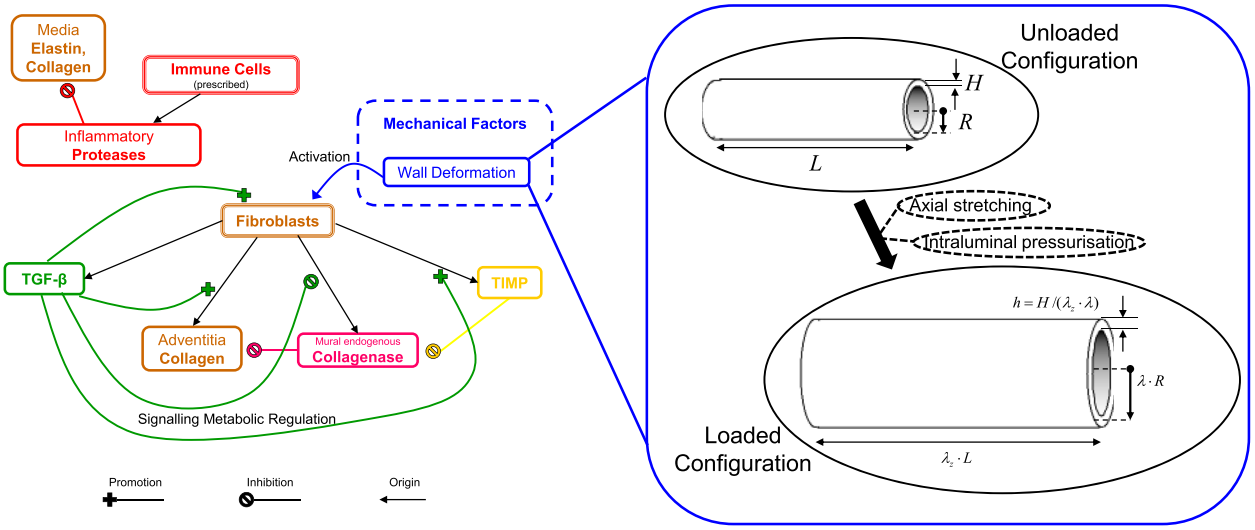

Fig. 1. Model components. Regulatory signalling pathways biochemical model component, *left*, interfacing with biomechanical model component, *right*.

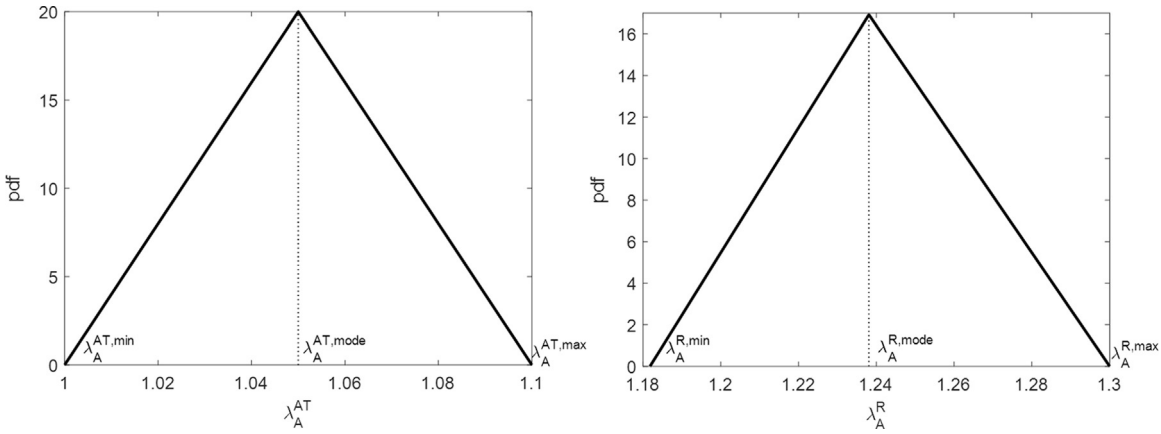

Fig. 2. Illustrative triangular probability density functions for adventitial collagen attachment stretch $\lambda_A{}^{AT}$ (*left*) and corresponding adventitial collagen recruitment stretch $\lambda_A{}^{R}$ (*right*) assuming a systolic circumferential stretch of 1.3.

2.2. Model formulation II: Signalling pathways biochemical model

The temporal evolution of cellular and molecular species involved in arterial connective tissue metabolism is modelled in this signalling pathways' biochemical model component, see diagram in Fig. 3. A system of coupled non-linear constant rate ODEs governs the cellular number densities n, molecular concentrations c and mass densities m normalised to the beginning of simulation (hereafter "normalised densities"). The arterial wall is reduced biochemically to two compartments: the media, constituted of fibrillar elastin and collagen; and the adventitia, where collagen metabolism is mediated by resident fibroblasts and the active molecular species they secrete. Parameter definitions, values and supporting references can be found in Appendix A.3.

2.2.1. Medial degeneration

Infiltrating immune cells such as macrophages or neutrophils are common findings within the wall of aneurysms (Rizas et al., 2009). The level of immune cells $n_M^i(t)$ in our model is prescribed, i.e.

$$n_M^i(t) = \begin{cases} i_0 & t < t_{i0} \\ i_0 + \left(\dfrac{t-t_{i0}}{k_i+(t-t_{i0})}\right)\cdot i_{\max} & t \geq t_{i0} \end{cases}. \tag{7}$$

The inflammatory response mediated by these cells is known to be involved in the degradation of medial elastin ($m_M{}^E$) and collagen ($m_M{}^C$) (Frösen et al., 2012). This process is simulated in the model by the dependence on immune cell-produced elastin-degrading proteases (elastases) $c_M{}^{pe}$ and collagen-degrading proteases (collagenases) $c_M{}^{pc}$ in the sink terms of the governing ODEs below:

$$\frac{dm_M^E}{dt} = -r_e \cdot c_M^{pe} \cdot m_M^E \quad \frac{dm_M^C}{dt} = -r_{cm} \cdot c_M^{pc} \cdot m_M^C \tag{8}$$

The governing ODEs for protease concentration are

$$\frac{dc_M^{pc}}{dt} = r_{pc_1} \cdot n_M^i - r_{pc_2} \cdot c_M^{pc} \quad \frac{dc_M^{pe}}{dt} = r_{pe_1} \cdot n_M^i - r_{pe_2} \cdot c_M^{pe}. \tag{9}$$

2.2.2. Adventitial collagen growth

The main cells responsible for collagen maintenance in the adventitia are fibroblasts; we denote their normalised number density as $n_A{}^F$. Fibroblasts produce (adventitial) procollagen ($c_A{}^P$) and zymogen ($c_A{}^z$) which are subsequently converted into active forms, i.e. collagen $m_A{}^C$ and collagenase $c_A{}^{ca}$, respectively (Shoulders and Raines, 2009; Siefert and Sarkar, 2012). Tissue Inhibitors of MetalloProteinases (TIMPs), denoted ($c_A{}^I$), are common collagenase inhibitors secreted by fibroblasts, which form an irreversible inhibitory complex with the enzymes and suppress their action (Brew et al., 2000). Collagen maintenance is a tightly regulated process. For instance, TGF-β is a signalling molecule with a collagen-promoting (i.e., *profibrotic*) action in the adventitia: it promotes procollagen synthesis (Lindahl et al., 2002); it stimulates fibroblast population expansion via increased migration (Martin et al., 1992), proliferation (Streuli et al., 1993; Akhurst and Hata, 2012) and differentiation (McAnulty, 2007); it suppresses zymogen secretion (Akhurst and Hata, 2012); it upregulates TIMP secretion (Akhurst and Hata, 2012). This molecule is secreted by fibroblasts in an inactive latent form $c_A^{\beta l}$, which is then activated to c_A^{β}. The system of ODEs governing collagen regulation is:

$$\frac{dn_A^F}{dt} = \left(r_{f_1} + r_{f_2} \cdot c_A^{\beta}\right) \cdot n_A^F - r_{f_3} \cdot n_A^F \tag{10}$$

$$\frac{dc_A^P}{dt} = \left(r_{p_1} + r_{p_2} \cdot c_A^{\beta}\right) \cdot n_A^F - r_{p_3} \cdot c_A^P \tag{11}$$

$$\frac{dm_A^C}{dt} = r_{c_1} \cdot c_A^P - r_{c_2} \cdot c_A^{ca} \cdot m_A^C \tag{12}$$

$$\frac{dc_A^z}{dt} = \left(\frac{r_{z_1}}{1+r_{z_2} \cdot c_A^{\beta}}\right) \cdot n_A^F - r_{z_3} \cdot c_A^z \tag{13}$$

$$\frac{dc_A^{ca}}{dt} = r_{ca_1} \cdot c_A^z - \left(r_{ca_2} + r_{ca_3} \cdot c_A^I\right) \cdot c_A^{ca} \tag{14}$$

$$\frac{dc_A^I}{dt} = \left(r_{I_1} + r_{I_2} \cdot c_A^{\beta}\right) \cdot n_A^F - \left(r_{I_3} + r_{I_4} \cdot c_A^{ca}\right) \cdot c_A^I \tag{15}$$

2.2.3. Regulatory signalling: TGF-β

TGF-β is one of the most significant regulators of collagen metabolism and matrix deposition in the arterial wall (Streuli et al., 1993). There is no baseline production of latent TGF-β by fibroblasts (Shi et al., 1996). Instead of being continuously present, it transiently acts as a link in fibroblast mechanotransduction regulatory signalling pathways, by coupling deviations from mechanical homeostasis to altered arterial collagen metabolism (Lindahl et al., 2002). We model the latent ($c_A^{\beta l}$) and active (c_A^{β}) forms of TGF-β as follows:

$$\frac{dc_A^{\beta l}}{dt} = \left(\frac{r_{\beta l_1} \cdot c_A^{\beta} + r_{\beta l_2} \cdot f\left(\lambda^F\right)}{1+r_{\beta l_3} \cdot m_A^C}\right) \cdot n_A^F - \left(r_{\beta l_4} + r_{\beta l_5} \cdot f\left(\lambda^F\right) \cdot n_A^F\right) \cdot c_A^{\beta l} \tag{16}$$

$$\frac{dc_A^{\beta}}{dt} = \left(r_{\beta_1} + r_{\beta_2} \cdot f\left(\lambda^F\right) \cdot n_A^F\right) \cdot c_A^{\beta l} - r_{\beta_3} \cdot c_A^{\beta} \tag{17}$$

TGF-β-mediated mechanotransduction is considered to take place at two levels. First, increased stretch of fibroblast cells above homeostatic values ($\lambda^F > \lambda_h^F$) leads to the increased production of latent TGF-β (O'Callaghan and Williams, 2000). Secondly, latent TGF-β is activated not only by endogenous and immune cell-driven proteolysis but also by a strain-dependent mechanism (Shi et al., 2011). To simulate this, for illustration, we consider $f\left(\lambda^F\right) = (\lambda^F - \lambda_h^F)/\lambda_h^F$ and, here, further assume that (i) the stretch fibroblasts transduce and respond to is equal to the stretch of the surrounding collagen fibres, and in particular $\lambda^F = \lambda_A^{C,\max}$; (ii) the homeostatic stretch target for fibroblasts λ_h^F is equal to the stretch target for the collagen fibres they remodel, the attachment stretch, $\lambda_h^F = \lambda_A^{AT,\max}$.

2.2.4. Collagen remodelling I: the attachment stretch distribution

During aneurysm enlargement, the adventitial collagen matrix may change its role from a protective sheath to playing a load-bearing role. The evolution of this tissue-level property is necessarily mediated by vascular cells, which compact newly deposited collagen into a strained state (Alberts et al., 1994), the "attachment" (Watton et al., 2004) or "deposition" (Bellini et al., 2014) stretch. We assume that (1) fibroblast cells continuously transduce the mechanical state of the collagen fibres (Chiquet et al., 2003); (2) fibroblast cell properties gradually change in response to changes in the mechanical properties of their surroundings; (3) cells have a finite memory, and thus the history of change in the mechanical condition of their surrounding tissue will influence their properties back to a certain time. Following from the previous assumptions, modelling the maximum attachment stretch as a running temporal average of the maximum collagen fibre stretch is a natural choice,

$$\lambda_A^{AT,\max}(t) = \frac{1}{T_{AT}} \cdot \left(\int_{t-T_{AT}}^{t} \lambda_A^{C,\max}|_{sys}(\tau)\, d\tau\right), \tag{18}$$

where T_{AT} is the length of the time interval over which the maximum adventitial collagen fibre stretch (at systole), $\lambda_A^{C,\max}|_{sys}$, is averaged. We then suppose that the

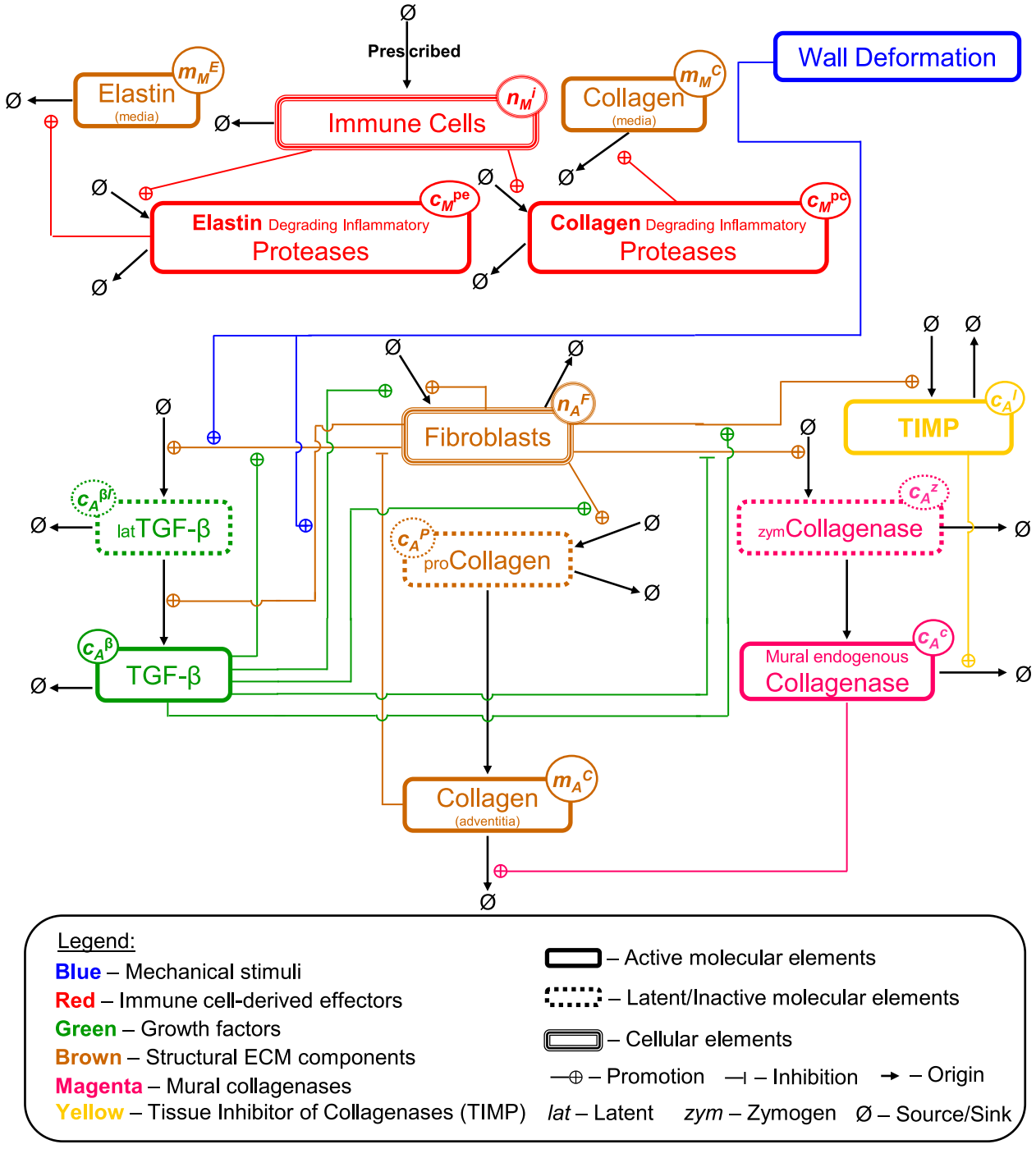

Fig. 3. Signalling pathways biochemical model diagram. All links between species included are based on published experimental observations. Variable symbols used in the governing equations can be found within circles next to the name of each species in the diagram. For details see text. (For interpretation of the references to colour in this figure caption, the reader is referred to the web version of this paper.)

minimal attachment stretch evolves according to

$$\lambda_A^{AT,\min}(t) = \lambda_A^{AT,\max}(t) - w(t)\,, \tag{19}$$

where $w(t)$ relates to the width of the attachment stretch distribution, which may narrow over time. Lastly, the modal attachment stretch evolves as

$$\lambda_A^{AT,mode}(t) = \lambda_A^{AT,\min}(t) + s(t)\cdot\left(\lambda_A^{AT,\max}(t) - \lambda_A^{AT,\min}(t)\right), \tag{20}$$

where $s(t)$ relates to the skew of the distribution, which may also evolve over time. In the examples presented in this paper and for simplicity, we take $w(t) = 0.1$ and $s(t) = 0.5$.

2.2.5. Collagen remodelling II: the recruitment stretch distribution

The distribution of collagen recruitment stretch in the adventitia $\lambda_A{}^R$ evolves to maintain the collagen stretch distribution towards the collagen attachment stretch distribution. Following Watton et al. (2004), the rate of evolution of minimum/mode and maximum recruitment stretches is driven by deviations of collagen stretch from homeostatic values (which are dynamic, cf. Eqs. (18)–(20)), i.e.

$$\frac{d\lambda_A^{R,\min}}{dt} = \alpha_A^C(n_A^F, m_A^C, c_A^{ca})\cdot\left(\frac{\lambda_A^{C,\max}|_{sys} - \lambda_A^{AT,\max}}{\lambda_A^{AT,\max}}\right) \tag{21}$$

$$\frac{d\lambda_A^{R,\max}}{dt} = \alpha_A^C(n_A^F, m_A^C, c_A^{ca})\cdot\left(\frac{\lambda_A^{C,\min}|_{sys} - \lambda_A^{AT,\min}}{\lambda_A^{AT,\min}}\right) \tag{22}$$

$$\frac{d\lambda_A^{R,mode}}{dt} = \alpha_A^C(n_A^F, m_A^C, c_A^{ca}) \cdot \left(\frac{\lambda_A^{C,mode}|_{sys} - \lambda_A^{AT,mode}}{\lambda_A^{AT,mode}} \right), \quad (23)$$

where $\alpha_A^C(n_A^F, m_A^C, c_A^{ca})$ is a rate parameter proportional to: the ratio of the levels of fibroblasts $n_A{}^F$ (which remodel the tissue) to collagen m_A^C being remodelled; the geometric mean of the levels of mural collagenases $c_A{}^{ca}$ (metabolising collagen) and the collagen being metabolised, i.e.

$$\alpha_A^C(n_A^F, m_A^C, c_A^{ca}) = \alpha_{A_0}^C \cdot \left(\frac{n_A^F}{m_A^C} \right) \cdot \sqrt{m_A^C \cdot c_A^{ca}}, \quad (24)$$

where $\alpha_{A_0}^C$ is a constant. The collagen recruitment stretch distribution in the media follows the same G&R laws, with corresponding parameter $\alpha_M^C = \alpha_{M_0}^C$ being constant, as collagen, collagenase and fibroblasts levels are not modelled in this layer.

2.3. Computational implementation

2.3.1. Parameter value selection

Parameter definitions and values can be found in Appendix A.3. They are chosen to qualitatively reflect experimental observations and balancing of source/sink terms at unperturbed conditions. The simulation time scale loosely resembles the life time of a human being; values for parameters controlling the G&R dynamics of the system ($\alpha_{M0}{}^C$, $\alpha_{A0}{}^C$, T_{AT}) are determined such that mechanical and biochemical variables achieve physiologically consistent steady states, e.g. $2 \le \lambda^{sys} \le 3$ and $\lambda_A^{C,max} \le 1.1$ (λ^{sys}: circumferential stretch at systole).

Initial conditions for the mechanical variables are as follows. Circumferential stretch at systole $\lambda_0{}^{sys}$ is initialised to 1.3 and the axial stretch is taken to be $\lambda_z = 1.3$ (constant throughout simulation). The initial attachment stretch distributions are prescribed; this implies initial values for the recruitment stretch distributions. More specifically, the adventitia is assumed to bear no load at systole $\lambda_A^{AT,max} = 1$. Furthermore, the distribution is assumed to be symmetric and with width $w(t) = 0.1$, so that $\lambda_A^{AT,min} = 0.9$ and $\lambda_A^{AT,mode} = 0.95$. It is assumed that the medial collagen bears load during the cardiac cycle and we suppose $\lambda_M^{AT,max} = 1.1$, the distribution is assumed to be symmetric and with width $w(t) = 0.1$ so that $\lambda_M^{AT,min} = 1$ and $\lambda_M^{AT,mode} = 1.05$. Determination of other material constants follows Watton et al. (2004). The densities of cellular and molecular species are normalised to their initial value. However, for species normally absent from arteries under baseline conditions, i.e. both forms of TGF-β ($c_A^{\beta l}$, c_A^{β}) and infiltrating immune cells ($n_M{}^i$), the initial values are set to zero.

2.3.2. Simulation loop

The general CMB model was implemented in Matlab R2013a (The Mathworks, Nattick, Ma, USA). The system of coupled equations was iteratively solved by a fully explicit approach: the system of ODEs (Eqs. (8)–(17) and Eqs. (21)–(23)) was solved by a backward finite differences Euler method using a fixed step length of 0.0069 years (at which step independence was achieved), while the algebraic force-balance equation (FBE) (Eq. (1)) was solved by `fzero`. Once system variables are initialised, simulation is started. The FBE is solved at systolic pressure for tissue and collagen fibre stretches; these mechanical quantities are passed to the mechanotransduction functionals, which are used to generate updated estimates of the cellular and biochemical variables and structural fibre distributions by means of the signalling pathways set of coupled ODEs. The updated estimates for the masses of load-bearing constituents and collagen recruitment stretches are input back into the FBE, which is solved again, iteratively. For comparison with previously published models, the conceptual model of Watton et al. (2009) is also implemented and simulated. See Appendix A.2 for details.

3. Results

We illustrate the application of the model to simulate the evolution of inflammatory aneurysms (IAs), Study 1, and the effects of a collagen-promoting drug on the development of this disease, Study 2. An initially healthy model of an artery is subject to a prescribed immune cell infiltration, Eq. (7). The ability of the model to simulate a return to a stable (*homeostatic*) state is then assessed.

3.1. Study 1: Inflammatory arterial aneurysm modelling

3.1.1. Mechanical variables

Fig. 4 displays the biomechanical evolution of an idealised aneurysm in response to prescribed infiltration of immune cells starting at $t = 40$ years. The production of proteolytic enzymes by these cells, Eq. (9), results in medial elastin degradation and arterial enlargement, as can be seen by the increase in circumferential stretch, Fig. 4a. Increasingly more of the load previously borne by medial elastin is now borne by adventitial collagen, leading to an increase in adventitial collagen stretch, Fig. 4c. The adventitia responds to this aneurysmal expansion by *growth*, increasing collagen mass (Fig. 4b), and *remodelling*, a change in attachment stretch distribution. This adaptive response of the adventitia slows down the enlargement of the artery, cf. reducing slope of each curve in Fig. 4a. At the end of the simulation, the circumferential stretch increases by a factor of 2–3 (Fig. 4a), and the collagen density increases by up to 50% (Fig. 4b). Notably, the adventitia changes its role from a protective sheath to bearing load (Fig. 4c), i.e. $\lambda_A^{C,max} = 1$ at $t = 0$ shifts to $\lambda_A^{C,max} > 1$ as the aneurysm converges to a new homeostasis. This adventitial adaptation was a result of the time-varying collagen attachment stretch law implemented in our model, Eq. (18), and emerges naturally from the underlying evolution of the collagen stretch distribution.

3.1.2. Target behaviours

Different rates of mechanical to biochemical mechanotransduction (*mechanotransduction sensitivity*) were simulated for the coupled CMB model. Each blue line (no markers) in Fig. 4 corresponds to a different value of rate constant $r_{\beta l_2}$ in Eq. (16), the rate of production of latent TGF-β by fibroblasts as a result of a deviation of collagen fibre stretch from its homeostatic target (the *attachment stretch*). It is clear that faster rates of mechanotransduction (solid and dashed lines) lead to faster and ultimately larger collagen production as a result of arterial expansion (Fig. 4b). Such fast re-enforcement of the adventitia halts further expansion, and results in stable domains (later time points in Fig. 4a and c). On the other hand, in the two slower mechanotransduction cases (dotted and dash-dotted lines) there are only very modest collagen increases in the adventitia (Fig. 4b), which cannot stop the continuous enlargement of the artery (later time points in Fig. 4a and c).

3.1.3. Cellular and molecular variables

Fig. 5 displays the predicted evolution of the cellular and biomolecular variables for simulation case $r_{\beta l_2} = 5$. The rates of change of these species are given by the equations in Section 2.2, a mathematical implementation of the biochemical network in Fig. 3. The prescribed immune cell infiltration (thick red line, circle markers) is followed by a similar increase in proteases (thin red line, circle markers). These proteolytic enzymes lead to degradation of medial elastin and collagen (dot-dashed brown line, no markers) and the artery enlarges, see Fig. 4a. Adventitial fibroblasts respond via TGF-β signalling, increasing the levels of its latent form (dashed green line, square markers) that is then converted into the active form (solid green line, square markers). As described in Section 2.2, TGF-β promotes collagen deposition by its multiple actions on fibroblasts: increase in fibroblast numbers (thick brown line, no markers), down-regulation of endomural collagenases (solid magenta line, upward triangle markers) and increase in inhibitors of collagenases or TIMPs (yellow line, downward triangle markers). The overall effect is an increase in collagen (thin brown line, no markers), also seen in Fig. 4b; such significant collagen *growth* leads to stabilisation of the aneurysm. This new mechanical homeostasis is perceived by fibroblasts, which reduce their TGF-β secretion. Finally and in the absence of this active agent, all biomolecules achieve a new steady-state, which is characterised by: an approximately 50% increase in fibroblasts, inhibitors, zymogen and procollagen; an approximately 25% increase in mature collagen and collagenase; a return of TGF-β levels to zero, which thus behaves as a transient mechanotransducer.

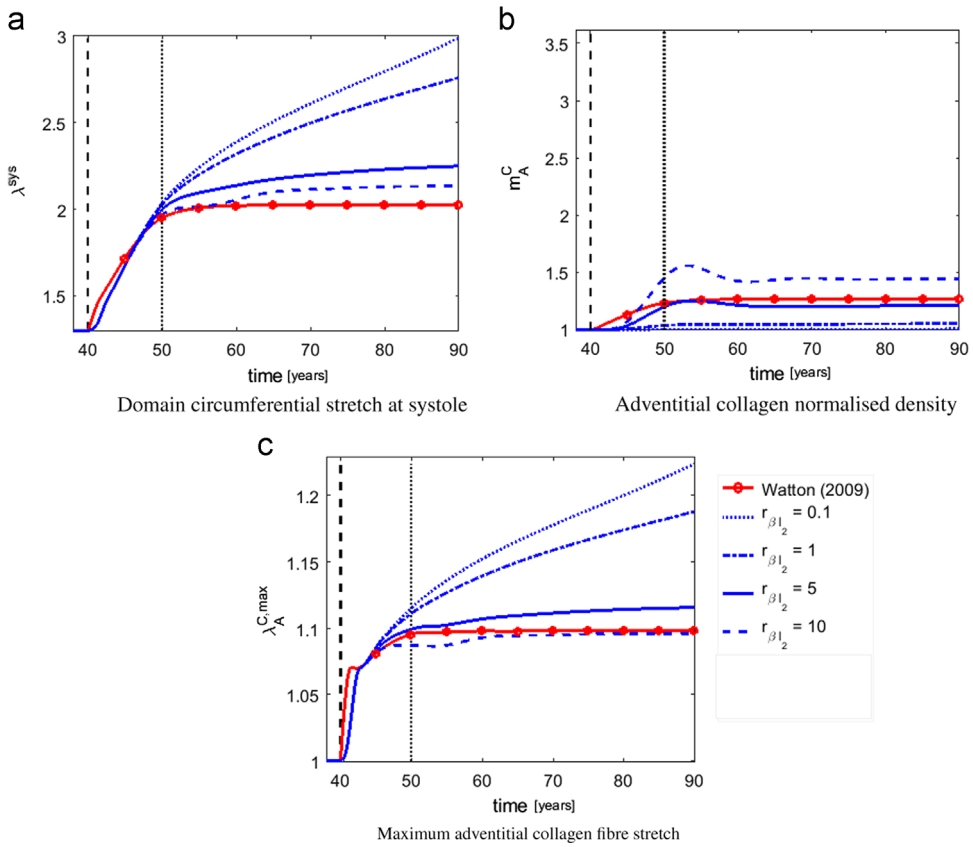

Fig. 4. IA modelling – parameter study results, mechanical variables. Infiltration of immune cells starts at $t = 40$ years (vertical black dashed line), follows Eq. (7) and results in almost complete degradation of medial elastin and collagen at $t = 50$ years (vertical black dotted line). The natural evolution of the mechanical variables characterising the system in response to such perturbation is plotted. Signalling pathways-coupled model (blue, no markers) $r_{\beta I_2} = 0.1$ (dotted), 1 (dash-dotted), 5 (solid), 10 (dashed) vs. Watton et al. (2009) (red, circle markers). (For interpretation of the references to colour in this figure caption, the reader is referred to the web version of this paper.)

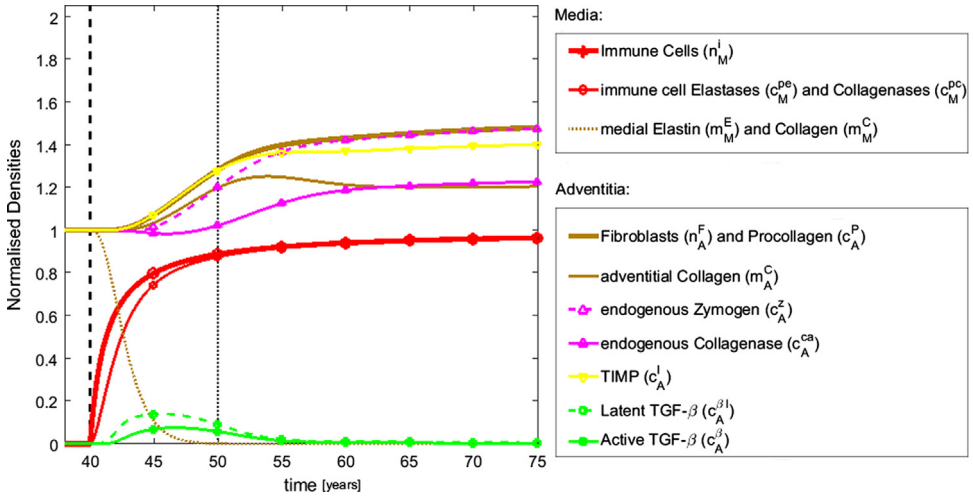

Fig. 5. IA modelling – parameter study results, cellular and biochemical variables. Infiltration of immune cells starts at $t = 40$ years (vertical black dashed line), follows Eq. (7) and results in almost complete degradation of medial elastin and collagen at $t = 50$ years (vertical black dotted line). The natural evolution of the cellular and biochemical quantities characterising the system in response to such perturbation is plotted until $t = 75$ years for the simulation case $r_{\beta I_2} = 5$. Key: immune cells (thick red solid line, circle markers), immune cell elastases/collagenases (thin red solid line, circle markers), fibroblasts and procollagen (thick brown solid line, no markers), adventitial collagen (thin brown solid line, no markers), medial collagen and elastin (brown dotted line, no markers), endogenous zymogenic/active collagenases (magenta dashed/solid lines, upward triangle markers), TIMP (yellow solid line, downward triangle markers), latent/active TGF-β (green dashed/solid lines, square markers). (For interpretation of the references to colour in this figure caption, the reader is referred to the web version of this paper.)

3.2. Study 2: Model application – TGF-beta therapy

Study 2 is identical to the previous study, except that a step increase in active TGF-β levels is introduced at $t_{Treat} = 45$ years. This collagen-promoting therapeutic strategy simulating TGF-β application by local delivery or gene-therapy has been suggested in the literature as potentially protective against aneurysm development (Ruddy et al., 2008).

3.2.1. Mechanical variables

The introduction of a TGF-β step has a dramatic effect on the evolution of system biomechanical variables, Fig. 6. Shortly after TGF-β is supplied at $t=45$ years, there is a very large increase in adventitial collagen levels, Fig. 6b, which over-shoots and then converges to 1.8–2.7 times initial levels. This large additional increase in adventitial collagen significantly constrains the expansion of the artery, with all simulation cases reaching stabilisation, Fig. 6, at much lower collagen

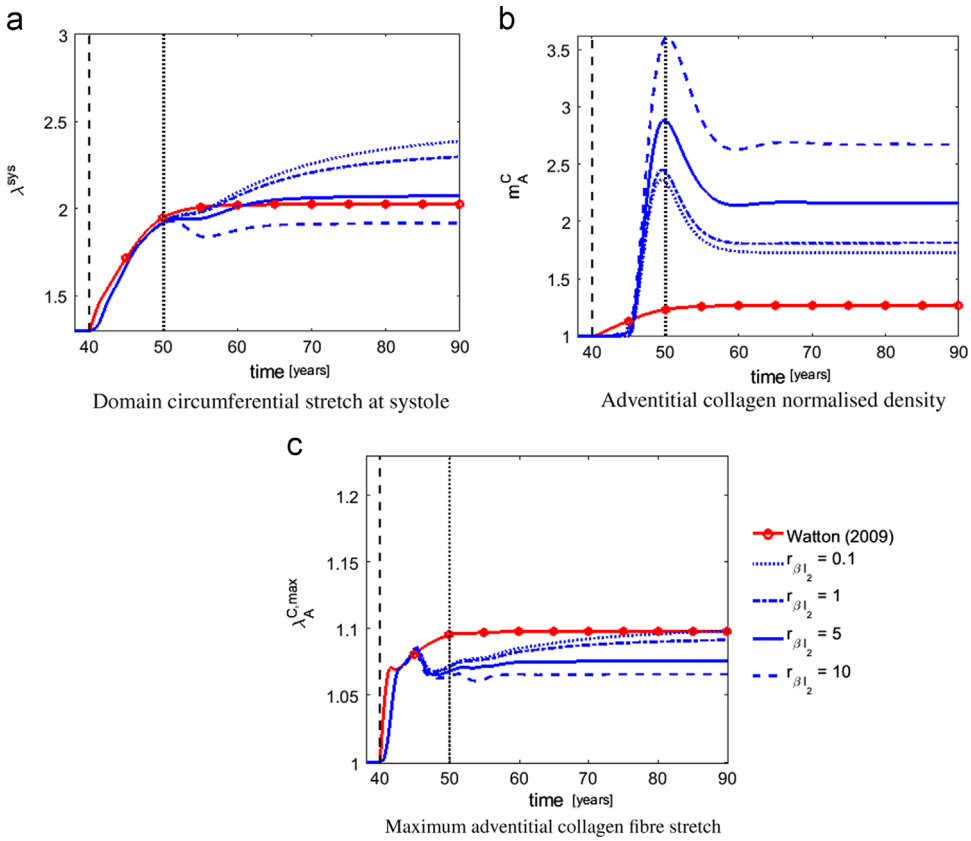

Fig. 6. TGF-β therapy – parameter study results, mechanical variables. Infiltration of immune cells starts at $t=40$ years (vertical black dashed line), follows Eq. (7) and results in almost complete degradation of medial elastin and collagen at $t=50$ years (vertical black dotted line). The response of the mechanical variables characterising the system following the application of a therapeutic step increase in active TGF-β normalised density at $t=45$ years is plotted. Signalling pathways-coupled model (blue, no markers) $r_{\beta I_2}=0.1$ (dotted), 1 (dash-dotted), 5 (solid), 10 (dashed) vs. Watton et al. (2009) (red, circle markers). (For interpretation of the references to colour in this figure caption, the reader is referred to the web version of this paper.)

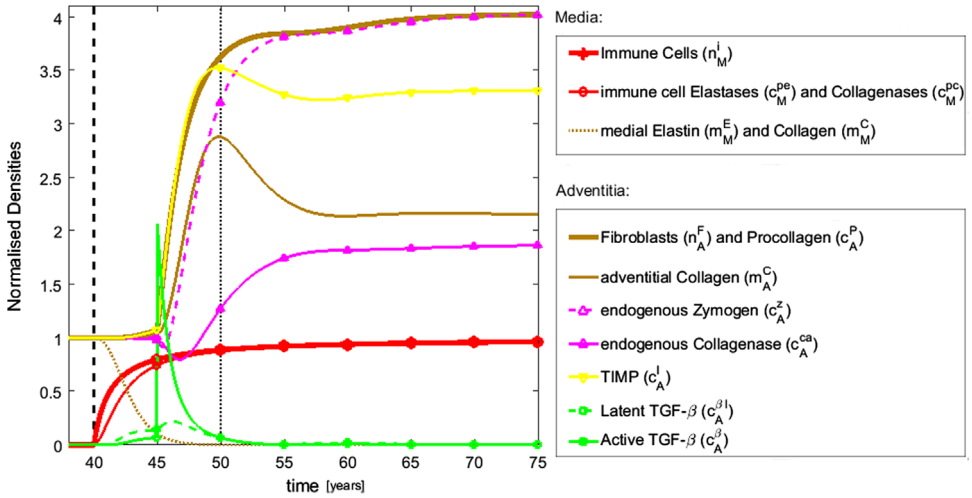

Fig. 7. TGF-β therapy – parameter study results, cellular and biochemical variables. Infiltration of immune cells starts at $t=40$ years (vertical black dashed line), follows Eq. (7) and results in almost complete degradation of medial elastin and collagen at $t=50$ years (vertical black dotted line). The response of the cellular and biochemical quantities characterising the system following the application of a therapeutic step increase in active TGF-β normalised density at $t_{Treat}=45$ years is plotted until $t=75$ years for the simulation case $r_{\beta I_2}=5$. Key: immune cells (thick red solid line, circle markers), immune cell elastases/collagenases (thin red solid line, circle markers), fibroblasts and procollagen (thick brown solid line, no markers), adventitial collagen (thin brown solid line, no markers), medial collagen and elastin (brown dotted line, no markers), endogenous zymogenic/active collagenases (magenta dashed/solid lines, upward triangle markers), TIMP (yellow solid line, downward triangle markers), latent/active TGF-β (green dashed/solid lines, square markers). (For interpretation of the references to colour in this figure caption, the reader is referred to the web version of this paper.)

stretches, Fig. 6c. When compared to the previous study, Fig. 6a, our coupled CMB model seems to suggest that a pharmacological-based collagen-promoting therapy leads to stabilisation of otherwise enlarging arteries (slower mechanotransduction cases), and faster stabilisation at lower stretches of already stabilising arteries (faster mechanotransduction cases).

3.2.2. Cellular and molecular variables

Fig. 7 shows the predicted evolution of cellular and biochemical quantities. As in the previous study, the increase in immune cells is prescribed (thick red curve, circle markers), leading to increased proteolytic enzymes (thin red curve, circle markers) and elastin degradation (dotted brown curve, no markers). A step in active TGF-β is introduced at $t_{Treat} = 45$ years (vertical solid green curve, square markers). The collagen-promoting actions of this signalling molecule take place as before (upregulation of fibroblast numbers, procollagen and inhibitors, downregulation of zymogen collagenase), but now to a much larger extent. As mechanical homeostasis is quickly reached (Fig. 6a), the levels of active TGF-β drop back to zero. A biochemical steady-state follows, characterised by a particularly large normalised density of fibroblasts (4 times larger than baseline), inhibitors (3.3 times) and collagen (over 2 times), as would be expected in a fibrotic tissue.

4. Discussion

4.1. Model insight

We have developed a novel Chemo-Mechano-Biological (CMB) mathematical model of arterial growth and remodelling (G&R) by coupling the conceptual aneurysm model of Watton et al. (2009) with the biochemical model of Dale et al. (1996). The underlying biological mechanisms included in the signalling pathways model component (Section 2.2), all of which supported or informed by experimental observations, have as their most significant components: (a) active molecules responsible for collagen metabolism (proteases and enzymatic inhibitors); (b) TGF-β, a potent regulator of fibroblast phenotype and matrix deposition that acts as a mechanotransduction signal for vascular cells; (c) fibroblasts, the dominant cell population in the adventitial layer and responsible for collagen metabolism; and (d) infiltrating immune cells, commonly found within the arterial wall in inflammatory aneurysms and atherosclerosis. Including this additional biological complexity allows our CMB model to capture arterial properties that emerge from the close bidirectional coupling between mechanics and chemo-biology, such as the effects of pharmacological therapy on the mechanical and biochemical condition of diseased arteries.

Aneurysms are known to display two distinct behaviours: stabilisation versus enlargement (sometimes alternating over time) (Sakalihasan et al., 2005). Understanding which arteries stabilise and should be left untreated vs. which vessels progressively enlarge and require intervention is of great clinical relevance. As was seen in Study 1, Fig. 6a in Section 3.1, our CMB model was able to capture both a return to mechanical and biochemical steady state (*stabilisation*), and a continuous enlargement for different rates of mechanotransduction. Aneurysm enlargement is extremely complex and multi-factorial; in any case, both experimental (Frösen et al., 2012) and computational (Wilson et al., 2013) studies suggest that the dynamics of collagen G&R and those of aneurysm enlargement are closely related. Furthermore, the new steady state achieved after the prescribed perturbation (immune cell infiltration) was characterised by trends qualitatively consistent with those seen in aneurysmal tissue: increased immune cell (Rizas et al., 2009) and (myo)fibroblast (Maiellaro and Taylor, 2007) numbers; reduced medial elastin (Sakalihasan et al., 2005) and increased adventitial collagen (Sakalihasan et al., 2005; Hobeika et al., 2007); increased TGF-β levels (Ruddy et al., 2008; Rizas et al., 2009); increased collagenase levels (Hobeika et al., 2007; Maiellaro and Taylor, 2007; Rizas et al., 2009); and increased TIMP concentration (Ruddy et al., 2008).

Promisingly, the model predicts that introducing a pharmacological collagen-promoting "therapy" in Study 2, i.e. applying a step increase in active TGF-β, acts to stabilise aneurysms; this is consistent with some experimental observations in animal models of abdominal aneurysm (Dai et al., 2005, 2011), thus supporting the clinical hypothesis that administering TGF-β may be protective against aneurysm development under some conditions. The ability to capture the dynamics of pharmacological agents and their effects on arterial mechanobiological evolution is a valuable insight offered by our CMB model. In the future, we envisage that coupled models of this kind may be used to simulate in silico the effect of drugs on the mechanical condition of a diseased artery, thus assisting medical decision-making.

4.2. Limitations and future directions

We modelled the arterial wall as a bilayered non-linear elastic cylindrical membrane. The choice of parameter values used in our studies was illustrative to reproduce different target behaviours of arterial tissue evolution (stabilisation vs. continuous enlargement), subject to conditions for realistic results. Extension to a full 3-Dimensional model of the arterial wall, e.g. Aparicio et al. (2014), Grytsan et al. (2015), and Eriksson et al. (2014), is a natural development.

Biochemical complexity was simplified by grouping together many different biomolecular types into a few representative variables: the only signalling molecule considered was TGF-β, and in particular isoform 1, which is known to be one of the most significant regulators of ECM deposition (Streuli et al., 1993); c_A^I specifically represents TIMP-1; over 30 different types of MMPs (Rizas et al., 2009) were grouped into three representative categories; fibrillar collagen types I and III were treated together. Furthermore, not all actions of such molecules were modelled. In particular, TGF-β is an important regulator of inflammation: it is secreted by immune cells, acting on them by increasing their migration and promoting secretion of proteases (Rizas et al., 2009; Akhurst and Hata, 2012).

From the many cell types populating the arterial wall, our model only considered fibroblasts (which populate the increasingly important adventitial layer, Humphrey and Canham, 2000), and immune cells. Other cell types are also present in the arterial wall. Intimal Endothelial Cells (ECs) transduce wall shear stress, thus regulating both luminal permeability to immune cells (Conway and Schwartz, 2012) and wall tonus via medial vascular smooth muscle cells (VSMCs) active stress generation (Humphrey et al., 2007). An interesting conceptual model of VSMC stress generation coupled to EC vasoconstrictor/vasodilator activity exists in the literature (Baek et al., 2007); coupling this EC/VSCM model to our Chemo-Mechano-Biological model would be relatively straightforward, providing a comprehensive and integrated description of arterial wall mechanobiology. Finally, in the presence of TGF-β and mechanical tension, adventitial fibroblasts may differentiate into myofibroblasts, a highly secretory, contractile and migratory cell type recently implicated in the development of vascular diseases such as thoracic aortic aneurysms (Forte et al., 2010).

Several particular choices were made when coupling arterial mechanics to biochemistry in our model. First, distributions of collagen fibre (λ^C) and attachment (λ^{AT}) stretch were modelled by triangular pdfs, Eq. (5). Second, the attachment stretch distribution was made to evolve over time according to Eqs. (18)–(20). This was

based on the observations that the adventitia progressively changes its role in disease from a protective straitjacket to the main load-bearer, and that fibroblasts depositing and stretching collagen are highly plastic cells (Stenmark et al., 2006; McAnulty, 2007). Here and for the first time, the hypothesised change in collagen attachment stretch was not prescribed (Chen, 2014), but rather emerged from the evolution of the system. Third, deviations from mechanical homeostasis were coupled to fibroblast mechanotransduction by the stretch-based functional $f\left(\lambda_A^{C,\max}\right)$; alternative, e.g. stress-based (Baek et al., 2006) functionals could easily be accommodated by our model.

A major shortcoming in this model is admittedly the lack of quantitative validation, which is partially due to the current lack of experimental data suitable to fit mechanobiological models (Humphrey, 2008). Future model development will benefit from data from both in vitro models of vascular cell–matrix interaction (Bai et al., 2014) and animal models of vascular disease (Li et al., 2014).

5. Summary

We propose a novel Chemo-Mechano-Biological (CMB) mathematical model of arterial Growth and Remodelling, which features an innovative coupling between regulatory signalling pathways and tissue biomechanics. Our CMB model is able to simulate both stabilisation and continuous enlargement of arterial aneurysms. It is a model prediction that the application of a collagen-promoting drug is able to arrest aneurysm growth, which is consistent with experimental observations. We envisage that such in silico models have the potential to provide insight into the effects of pharmacological therapy on vascular disease and guide personalised treatment strategies.

Conflict of interest

The authors declare that there is no conflict of interest in this work.

Acknowledgements

Pedro Aparício holds a EPSRC Systems Biology Doctoral Training Centre studentship. The support is greatly acknowledged.

Appendix A. Supplementary data

Supplementary data associated with this paper can be found in the online version at http://dx.doi.org/10.1016/j.jbiomech.2016.04.037.

References

Akhurst, R.J., Hata, A., 2012. Targeting the TGFβ signalling pathway in disease. Nat. Rev. Drug Discov. 11 (10), 790–811.
Alberts, B., Bray, D., Lewis, J., Raff, M., Roberts, K., Watson, J., 1994. Molecular Biology of the Cell, 3rd edition. Garland Publishing, New York, p. 984.
Aparicio, P., Mandaltsi, A., Boamah, J., Chen, H., Selimovic, A., Bratby, M., Uberoi, R., 2014. Modelling the influence of endothelial heterogeneity on the progression of arterial disease: application to abdominal aortic aneurysm evolution. Int. J. Numer. Methods Biomed. Eng. 30, 563–586.
Baek, S., Rajagopal, K.R., Humphrey, J.D., 2006. A theoretical model of enlarging intracranial fusiform aneurysms. J. Biomed. Eng. 128, 142–149.
Baek, S., Valentin, A., Humphrey, J., 2007. Biomechanics of cerebral vasospasm and its resolution: II. Constitutive relations and model simulations. Ann. Biomed. Eng. 35 (9), 1498–1509.
Bai, Y., Lee, P.-F., Humphrey, J.D., Yeh, A.T., 2014. Sequential multimodal microscopic imaging and biaxial mechanical testing of living multicomponent tissue constructs. Ann. Biomed. Eng., 1–15.
Balakhovsky, K., Jabareen, M., Volokh, K., 2014. Modeling rupture of growing aneurysms. J. Biomech. 47 (3), 653–658.
Bellini, C., Ferruzzi, J., Roccabianca, S., Di Martino, E.S., Humphrey, J.D., 2014. A microstructurally motivated model of arterial wall mechanics with mechanobiological implications. Ann. Biomed. Eng. 42 (3), 488–502.
Brew, K., Dinakarpandian, D., Nagase, H., 2000. Tissue inhibitors of metalloproteinases: evolution, structure and function. Biochim. Biophys. Acta 1477 (1–2), 267–283.
Chen, H., 2014. Intracranial Aneurysm Disease: Novel Modelling of Inception and the Microstructural Adaption of Collagen Fabric (Ph.D. dissertation). University of Oxford.
Chiquet, M., Renedo, A.S., Huber, F., Flück, M., 2003. How do fibroblasts translate mechanical signals into changes in extracellular matrix production? Matrix Biol.: J. Int. Soc. Matrix Biol. 22 (1), 73–80.
Conway, D., Schwartz, M., 2012. Lessons from the endothelial junctional mechanosensory complex. F1000 Biol. Rep. 4 (January), 1.
Dai, J., Losy, F., Guinault, A.-M., Pages, C., Anegon, I., Desgranges, P., Becquemin, J.-P., Allaire, E., 2005. Overexpression of transforming growth factor-β1 stabilizes already-formed aortic aneurysms a first approach to induction of functional healing by endovascular gene therapy. Circulation 112 (7), 1008–1015.
Dai, J., Michineau, S., Franck, G., Desgranges, P., Becquemin, J.-P., Gervais, M., Allaire, E., 2011. Long term stabilization of expanding aortic aneurysms by a short course of cyclosporine a through transforming growth factor-beta induction. PloS One 6 (12), e28903.
Dale, P., Sherratt, J., Maini, P., 1996. A mathematical model for collagen fibre formation during foetal and adult dermal wound healing. Proc. R. Soc. London 263 (B), 653–660.
Eriksson, T., Watton, P., Luo, X., Ventikos, Y., 2014. Modelling volumetric growth in a thick walled fibre reinforced artery. J. Mech. Phys. Solids 73, 134–150.
Forte, A., Della Corte, A., De Feo, M., Cerasuolo, F., Cipollaro, M., 2010. Role of myofibroblasts in vascular remodelling: focus on restenosis and aneurysm. Cardiovasc. Res. 88 (3), 395–405.
Frösen, J., Tulamo, R., Paetau, A., Laaksamo, E., Korja, M., Laakso, A., Niemelä, M., Hernesniemi, J., 2012. Saccular intracranial aneurysm: pathology and mechanisms. Acta Neuropathol. 123 (6), 773–786.
Grytsan, A., Watton, P.N., Holzapfel, G.A., 2015. A thick-walled fluid–solid-growth model of abdominal aortic aneurysm evolution: application to a patient-specific geometry. J. Biomechan. Eng. 137 (3), 031008.
Hill, M.R., Duan, X., Gibson, G.A., Watkins, S., Robertson, A.M., 2012. A theoretical and non-destructive experimental approach for direct inclusion of measured collagen orientation and recruitment into mechanical models of the artery wall. J. Biomech. 45 (5), 762–771.
Hobeika, M.J., Thompson, R.W., Muhs, B.E., Brooks, P.C., Gagne, P.J., 2007. Matrix metalloproteinases in peripheral vascular disease. J. Vasc. Surg. 45 (4), 849–857.
Humphrey, J., Canham, P., 2000. Structure, mechanical properties, and mechanics of intracranial saccular aneurysms. J. Elast. 61, 49–81.
Humphrey, J., Baek, S., Niklason, L., 2007. Biochemomechanics of cerebral vasospasm and its resolution: I. A new hypothesis and theoretical framework. Ann. Biomed. Eng. 35 (9), 1485–1497.
Humphrey, J.D., 2008. Vascular adaptation and mechanical homeostasis at tissue, cellular, and sub-cellular levels. Cell Biochem. Biophys. 50 (2), 53–78.
Leask, A., 2010. Potential therapeutic targets for cardiac fibrosis tgfβ, angiotensin, endothelin, ccn2, and pdgf, partners in fibroblast activation. Circ. Res. 106 (11), 1675–1680.
Li, W., Li, Q., Jiao, Y., Qin, L., Ali, R., Zhou, J., Ferruzzi, J., Kim, R.W., Geirsson, A., Dietz, H.C., et al., 2014. Tgfbr2 disruption in postnatal smooth muscle impairs aortic wall homeostasis. J. Clin. Investig. 124 (2).
Lindahl, G.E., Chambers, R.C., Papakrivopoulou, J., Dawson, S.J., Jacobsen, M.C., Bishop, J.E., Laurent, G.J., 2002. Activation of fibroblast procollagen alpha 1 (I) transcription by mechanical strain is transforming growth factor-beta-dependent and involves increased binding of CCAAT-binding factor (CBF/NF-Y) at the proximal promoter. J. Biol. Chem. 277 (8), 6153–6161.
Lindsay, M.E., Dietz, H.C., 2011. Lessons on the pathogenesis of aneurysm from heritable conditions. Nature 473 (7347), 308–316.
Maiellaro, K., Taylor, W.R., 2007. The role of the adventitia in vascular inflammation. Cardiovasc. Res. 75 (4), 640–648.
Martin, P., Hopkinson-woolley, J., McCluskey, J., 1992. Growth factors and cutaneous wound repair. Prog. Growth Factor Res. 4, 25–44.
McAnulty, R., 2007. Fibroblasts and myofibroblasts: their source, function and role in disease. Int. J. Biochem. Cell Biol. 39, 666–671.
McDougall, S., Dallon, J., Sherratt, J., Maini, P., 2006. Fibroblast migration and collagen deposition during dermal wound healing: mathematical modelling and clinical implications. Philos. Trans. R. Soc. A: Math. Phys. Eng. Sci. 364 (1843), 1385–1405.
Montecucco, F., Mach, F., 2009. Atherosclerosis is an inflammatory disease. Semin. Immunopathol. 31 (1), 1–3.
O'Callaghan, C.J., Williams, B., 2000. Mechanical strain-induced extracellular matrix production by human vascular smooth muscle cells: role of TGF-β1. Hypertension 36, 319–324.
Rizas, K., Ippagunta, N., Tilson Jr., M.D., 2009. Immune cells and molecular mediators in the pathogenesis of the abdominal aortic aneurysm. Cardiol. Rev. 17, 201–210.

Ruddy, J.M., Jones, J.a., Spinale, F.G., Ikonomidis, J.S., 2008. Regional heterogeneity within the aorta: relevance to aneurysm disease. J. Thorac. Cardiovasc. Surg. 136 (5), 1123–1130.
Sakalihasan, N., Limet, R., Defawe, O.D., 2005. Abdominal aortic aneurysm. Lancet 365 (9470), 1577–1589.
Shi, Y., Brien, J.E.O., Brien, O., Fard, A., Zalewski, A., 1996. Transforming growth factor-β1 expression and myofibroblast formation during arterial repair. Arterioscler. Thromb. Vasc. Biol. 16, 1298–1305.
Shi, M., Zhu, J., Wang, R., Chen, X., Mi, L., Walz, T., Springer, T.a., 2011. Latent TGF-β structure and activation. Nature 474 (7351), 343–349.
Shoulders, M.D., Raines, R.T., 2009. Collagen structure and stability. Annu. Rev. Biochem. 78, 929–958.
Siefert, S., Sarkar, R., 2012. Matrix metalloproteinases in vascular physiology and disease. Vascular 20 (4), 210–216.
Stenmark, K.R., Fagan, K.a., Frid, M.G., 2006. Hypoxia-induced pulmonary vascular remodeling: cellular and molecular mechanisms. Circ. Res. 99 (7), 675–691.
Streuli, C., Schmidhauser, C., Kobrin, M., Bissel, M.J., Derinck, R., 1993. Extracellular matrix regulates expression of TGF-beta 1 gene. J. Cell Biol. 120, 253–260.
Volokh, K.Y., Vorp, D.A., 2008. A model of growth and rupture of abdominal aortic aneurysm. J. Biomech. 41, 1015–1021.
Warsinske, H.C., Ashley, S.L., Linderman, J.J., Moore, B.B., Kirschner, D.E., 2015. Identifying mechanisms of homeostatic signaling in fibroblast differentiation. Bull. Math. Biol., 1–27.
Watton, P.N., Hill, N.A., Heil, M., 2004. A mathematical model for the growth of the abdominal aortic aneurysm. Biomech. Model. Mechanobiol. 3 (2), 98–113.
Watton, P.N., Ventikos, Y., Holzapfel, G.A., 2009. Modelling the growth and stabilization of cerebral aneurysms. Math. Med. Biol. 26, 133–164.
Wilson, J., Baek, S., Humphrey, J., 2012. Importance of initial aortic properties on the evolving regional anisotropy, stiffness and wall thickness of human abdominal aortic aneurysms. J. R. Soc. Interface 9 (74), 2047–2058.
Wilson, J.S., Baek, S., Humphrey, J.D., 2013. Parametric study of effects of collagen turnover on the natural history of abdominal aortic aneurysms. Proc. R. Soc. A: Math. Phys. Eng. Sci., 469.